Hindawi
Science and Technology of Nuclear Installations
Volume 2024, Article ID 5565346, 12 pages
https://doi.org/10.1155/2024/5565346

Research Article

Accuracy Evaluation of Monte Carlo Simulation Results Using ENDF/B-VIII.0 and JENDL-5 Libraries for 10 MW_{th} Micro Heat Pipe-Cooled Reactor

Thanh Mai Vu [1,2,3] and Le Quang Linh Tran [3]

[1]*Department of Mechanical and Nuclear Engineering, University of Sharjah, P.O. Box, Sharjah 27272, UAE*
[2]*Research Institute of Sciences and Engineering, University of Sharjah, P.O. Box, Sharjah 27272, UAE*
[3]*VNU University of Science, Vietnam National University, 334 Nguyen Trai, Thanh Xuan, Hanoi 120-034, Vietnam*

Correspondence should be addressed to Le Quang Linh Tran; linhltq2101@gmail.com

Received 10 July 2023; Revised 7 March 2024; Accepted 13 March 2024; Published 8 April 2024

Academic Editor: Doddy Kastanya

The micro heat pipe-cooled reactor is an innovative type of reactor that utilizes heat pipes to cool its core. It consists of a reactor core, an energy conversion system, shielding, and a heat removal system. This reactor shows great potential as a viable option for supplying electricity in remote areas. By incorporating a monolithic core with heat pipes and an efficient heat conversion system, this reactor design eliminates the need for a main pipeline, circulating pump, and auxiliary equipment, resulting in a cost-effective, compact, and transportable system. The monolithic reactor design has undergone significant advancements in neutronics and thermal hydraulics. This article focuses on evaluating the impact of the latest released nuclear data libraries, ENDF/B-VIII.0 and JENDL-5, on calculated neutronics and kinetics parameters. The total k_{eff} uncertainty was propagated and found to be significant for both recently evaluated nuclear data libraries (678.52 pcm for ENDF/B-VIII.0 and 525.91 pcm for JENDL-5, respectively). The total uncertainty originated from nuclear data was evaluated for total ν, reaction cross sections, and angular distributions in the case of JENDL-5, and for ENDF/B-VIII.0, uncertainty from angular distributions was not included because of the unavailability of its multigroup structure covariance matrices. The results reveal that the largest contributor for ENDF/B-VIII.0 is ^{235}U total (409.18 pcm), while that for JENDL-5 is ^{56}Fe capture cross section (361.93 pcm). For the kinetic parameter's uncertainty, the impact on the total β_{eff}, l_{eff}, and λ_{eff} simulation results was found to be not significant (about 1%).

1. Introduction

Micro-reactors, which are also known as nuclear batteries due to their small size, can produce about 1 to 10 MWe, and each MWe can power approximately 1000 homes. The micro-reactors are being developed with the aim of achieving unattended operation, built-in safety, and the ability to start up without external assistance. They can be used for military bases, emergency cases, homes, and hospitals without depending on the power grids. Additionally, the compact size and lightweight nature of these systems guarantee flexibility in manufacturing and transportation. In this study, a new micro-reactor design that uses heat pipe technology for heat transfer known as micro heat pipe-cooled reactor (MHPR) is modelled and investigated. With the adoption of the heat pipe and efficient energy conversion system, the main pipeline and circulating pumps are simplified from the reactor core. It depends only on capillary action to pump the liquid. As a result, there are no moving parts that will reduce the noise level, are maintenance-free, and require no mechanical or electrical input, leading to lower operating costs. Moreover, these micro-reactors can operate for a long term without refuelling; each heat pipe works separately and is environmentally safe.

Originally, the research of the heat pipe reactor was promoted by space reactor applications. The design of the MHPR with a monolithic core has undergone significant advancements, particularly in neutronics and thermohydraulics investigation. By combining heat pipes and a solid block core, the MHPR operates as a "solid-state reactor" with minimal moving components, ensuring a reliable and long-lasting decentralized energy generator. The idea of the reactor concept was initially introduced at Los Alamos National Lab (LANL) several decades ago. Heat pipes are integrated into the lattice solid core, offering a novel approach to dissipate fission and decay heat. These heat pipes consist of a small quantity of working fluid enclosed within a sealed steel pipe and operate passively at pressures below atmospheric levels. The primary function of the heat pipes is to efficiently transfer heat from the evaporator section within the core to the condenser section outside, maintaining a continuous isothermal vapour/liquid internal flow. Multiple heat exchangers, including one for power conversion and two for redundant decay heat removal, can be accommodated in the condenser region [1]. The heat pipe working mechanism is illustrated in Figure 1.

In the LANL concept, the core was designed for 5 MW_{th} and the centre is made up of six pipe-shaped segments [3]. The operational and performance features and metrics of Idaho National Laboratory's new active core architectures were deliberately designed to be similar to the LANL concept. Each section is a tank with two walls. The heat pipes, fuel pins, spacer plates, and liquid metal sodium are all included in the inner tank; the sodium occupies the interstitial space between the heat pipes, fuel pins, and spacer plates. Despite the different active core design geometries, those designs are very similar in several aspects. Core weight, core size, heat pipe use, UO_2 fuel, in-core steel, high temperature, excess reactivity, neutron spectrum, burnup, and core lifetime are typical characteristics. Ex-core features and parts, such as the heat pipe configuration, power conversion unit, alumina side reflector, and the number of control drums, will remain essentially unchanged [4].

With the advantages of compact design, mobility, and relatively low operating cost, heat pipe reactors are a potential energy source for remote applications. As with many reactor design activities, heat pipe reactor performance is mainly investigated using simulation. In the Monte Carlo simulation, despite the geometrical aspect, the reliability of the calculation results depends on the number of histories (statistical uncertainty) and nuclear data. The statistical uncertainty typically varies as $1/\sqrt{N}$ $1/\sqrt{N}$, where N is the number of considered histories. Thus, when a sufficient number of histories are used, the contribution from the statistical uncertainty becomes minor and the main contribution to the simulation result uncertainty would be from the nuclear data. The uncertainties originating from nuclear data can be significant and affect the evaluation of the safety features of the designed system. Previous research findings raised concern about the significant impact of the inaccuracy of current evaluated nuclear libraries on simulation results of the fast reactor designs. Large discrepancies were found between the target accuracies of the effective multiplication factor (k_{eff}) [5] and the evaluated uncertainties for the fast system [6–9]. The simulation of a heat pipe reactor with a major difference in core arrangement, heat transfer mechanism, and material compositions has never been investigated to assess the impact of the nuclear data uncertainties on the simulation results. In particular, on a microsize reactor where the neutron leakage may have a large impact, angular distribution and its uncertainty would cause some impacts on calculation results. From that approach, the aim of the study is to propagate the uncertainty of some neutronics and kinetics parameters of MHPR and evaluate their reliability using the Monte Carlo simulation—Serpent 2 code [10] with ENDF/B-VIII.0 [11] and the latest nuclear data library JENDL-5 [12]. The model used in this study is the 10 MW_{th} MHPR core employing the basics of the monolith core concept in the above-mentioned design with compact size and enhanced safety features. The details of the calculation model are discussed in Section 2. The methodology and computer code used for core parameter calculations and uncertainty evaluation are presented in Section 3. The results of those parameters and their accuracy are discussed in Section 4. Finally, the conclusions are provided.

2. 10 MW_{th} MHPR Design

The simplified MHPR core configuration with a designated power of 10 MW_{th} includes a solid hexagonal block in which the fuel and the heat pipes are built in a lattice configuration (Figure 2(a)). The fission heat is exchanged to the heat pipes via the solid block, and the heat pipes transfer the heat to the energy conversion system. Therefore, the reactor size can be more compact and economical because no pipeline, pump, and auxiliary equipment are required. The active core height is 100 cm with 30 cm high upper and lower reflectors. A parameter survey on four different reflectors (aluminium oxide (Al_2O_3), beryllium (Be), beryllium oxide (BeO), and magnesium oxide (MgO)) was conducted to seek the highest reflector worth, which indicates the improvement in neutron economy. Reflector worth is the difference between k_{eff} with different reflecting materials and k_{eff} without any reflecting material. The result reveals BeO to be the best reflector material with the highest reflector worth (50502.00 pcm) and was chosen to be the reflector for the 10 MW_{th} MHPR. The vertical and horizontal cross sections of the reactor core are plotted by Serpent 2 code in Figure 2(a). The core diameter is 101 cm. Its size is about one-third that of commercial pressurized water reactors (PWRs). The outer hexagonal layer known as a monolith houses the heat pipes and the fuel with 2.024 cm pitch. A total of 2376 heat pipes with potassium (K) working fluid were employed to transfer the heat of 10 MW_{th} reactor core. The heat pipe inner diameter is 1.56 cm, while the wick diameter and heat pipe wall diameter are 1.76 cm and 1.86 cm, respectively. The heat pipe-to-heat pipe pitch is 2.02 cm. Figure 3 shows the horizontal sectional view of a heat pipe inside the active core region. Uranium dioxide (UO_2) with 19.75% of ^{235}U enrichment is used as fuel. Because Doppler's effect in the high-enriched uranium-fuelled monolithic reactor is minor, the reactivity

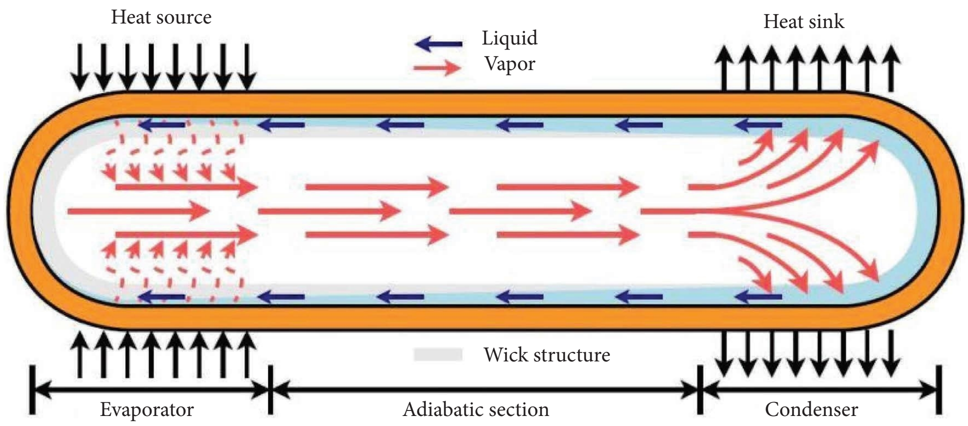

Figure 1: Heat pipe working mechanism [2].

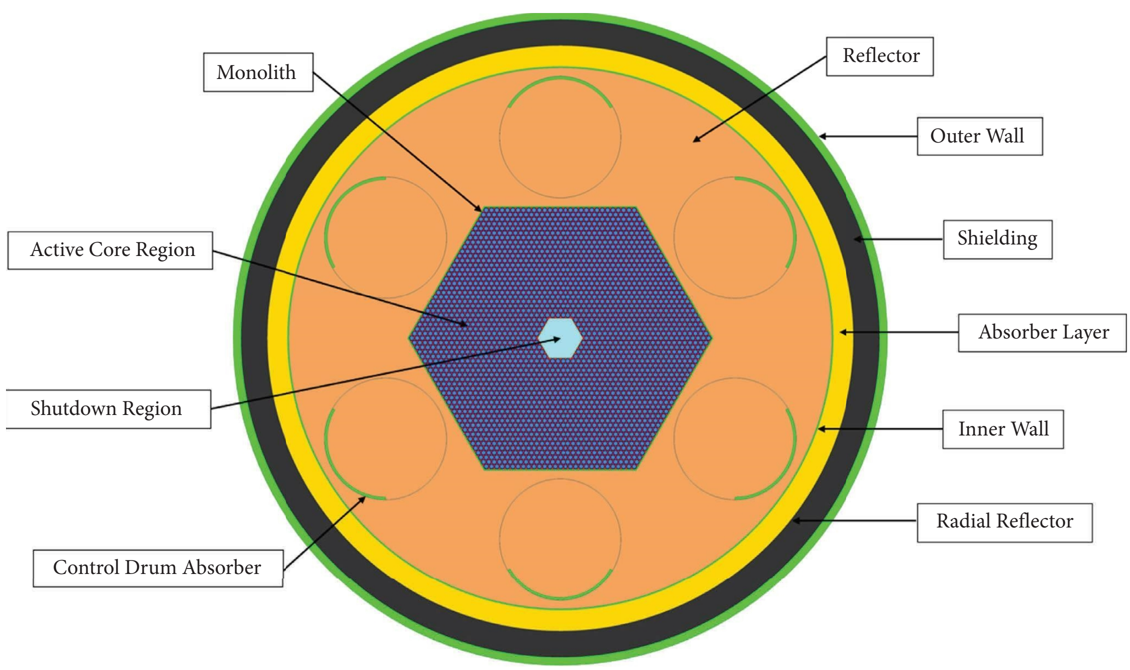

(a)

Figure 2: Continued.

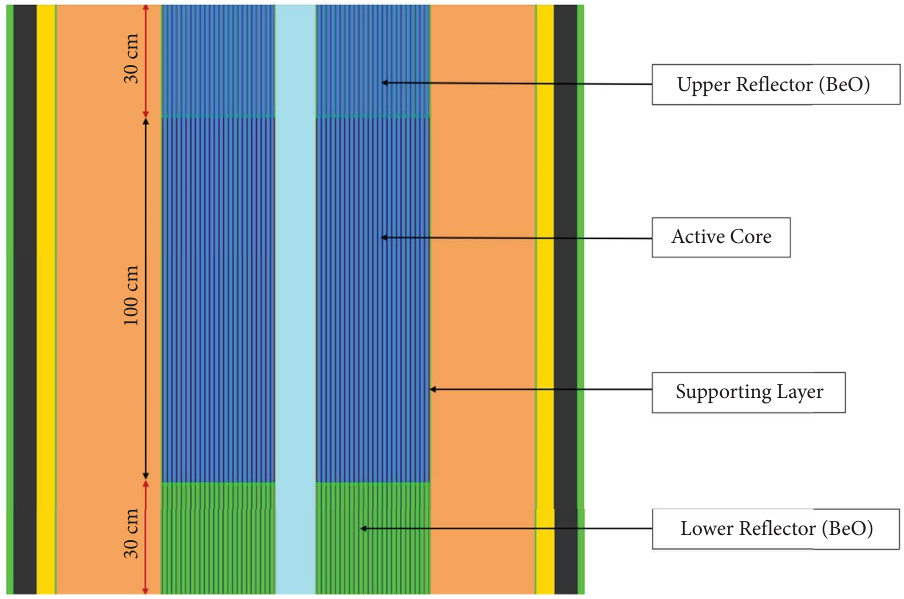

(b)

FIGURE 2: (a) Horizontal sectional view of the MHPR core. (b) Vertical sectional view of the MHPR core.

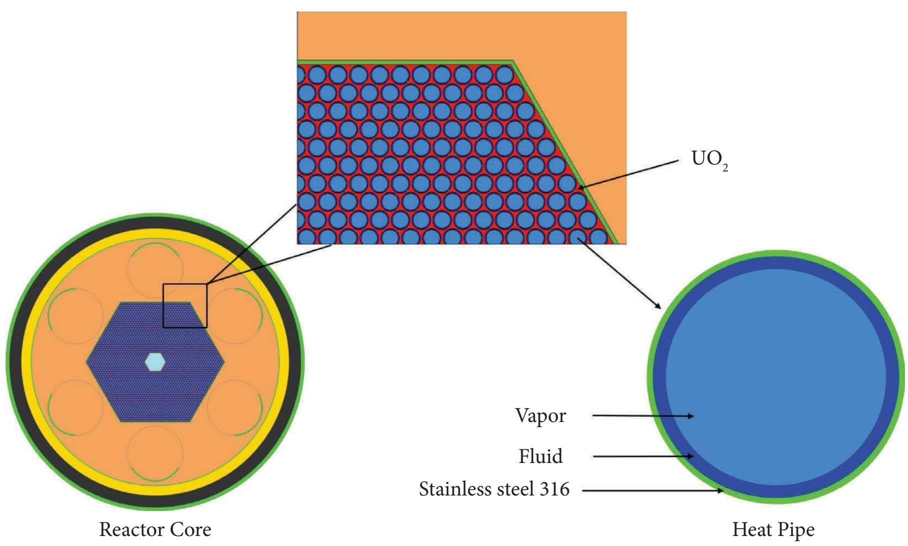

FIGURE 3: Horizontal sectional view of a heat pipe inside the active core region.

is regulated by thermal expansion and subsequent negative reactivity feedback and control rod drums [1]. The six control drums are used to control the criticality and the operation of the reactor. The control rod shutdown region, which is used for both normal operating conditions and any emergency case, is located in the core centre. The inner and outer walls are made of stainless steel 316. B_4C absorber and shielding are employed to shield the neutron leakage from the active core. The main parameters of 10 MW_{th} MHPR are listed in Table 1, and the neutron spectrum is depicted in Figure 4. The fast neutron spectrum of the system with the spectral weight of $0.1\,\text{MeV} < E < 1\,\text{MeV}$ energy region is about 70%.

3. Methodology and Calculation Tool

The main performance parameters of the MHPR core including effective multiplication factor, control drum worth, temperature reactivity feedback, and burnup calculations for 10 MW_{th} MHPR were obtained by Serpent 2 code using ENDF/B-VIII.0 and JENDL-5. A number of histories of 10^5 with 150 inactive cycles and 500 active cycles were used for the simulation. k_{eff} has a statistical error of less than 1.4×10^{-04}. β_{eff}, l_{eff}, and λ_{eff} were also achieved to reveal the core characteristics. In Serpent 2 calculation, the iterated fission probability (IFP) method [13, 14] was employed and the β_{eff}, l_{eff}, and λ_{eff} were achieved by the adjoint weighting.

Table 1: Main parameters of the 10 MW_{th} MHPR core.

Parameters	Value
Total power (MW_{th})	10 MW_{th}
Active height (cm)	100
Upper/lower reflector (cm)	30
Core diameter (d, cm)	250
Active core pitch (cm)	101
Fuel type	UO_2 (19.75% enrichment)
Fuel volume (cm^3)	205,944.1
Operating temperature (K)	1200
Number of heat pipes	2376
Heat pipe inner diameter (cm)	1.575
Heat pipe wick diameter (cm)	1.757
Heat pipe wall diameter (cm)	1.857
Heat pipe-to-heat pipe pitch (cm)	2.024
Reflector material	BeO

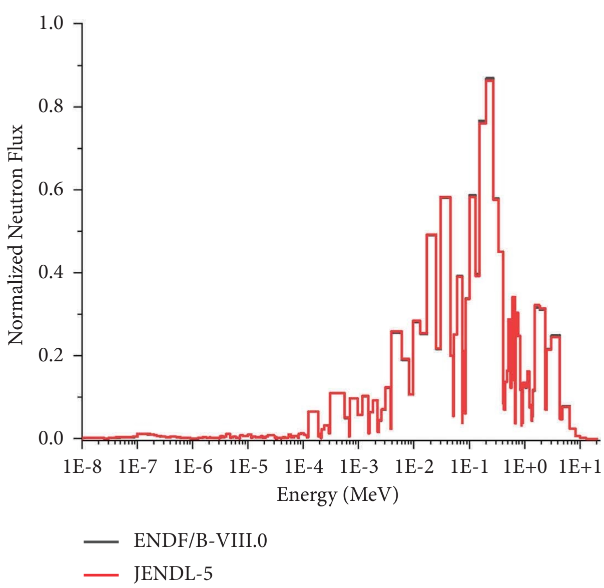

Figure 4: Neutron spectra of the MHPR.

The uncertainty for eigenvalue k_{eff}, control drum worth, and the kinetic parameters of 10 MW_{th} MHPR core are the subjects for the uncertainty analysis.

The ENDF/B-VIII.0 library, released in 2018, includes improved thermal 49 neutron scattering and new evaluated data for neutron reactions of H-1, O-16, 50 Fe-56, U-235, U-238, and Pu-239 [11]. It includes updated 51 data for light nuclei, structural materials, actinides, fission energy release, 52 prompt fission neutrons, and thermal neutron scattering data. The most recently released library, JENDL-5, consists of 11 sublibraries with improved data of neutron reactions. The number of evaluated nuclides was increased up to 795 nuclides, and the energy region was extended up to 200 MeV or 3 GeV for high-energy applications. JENDL-5 also adopted the originally evaluated data for fission yields and thermal scattering laws. For uranium-fuelled reactors, it is noteworthy that, for $^{235,238}U$ and ^{239}Pu, JENDL-5 also employed the resonance parameter of CIELO as ENDF/B-VIII. However, some adjustments have been made on their elastic scattering, fission, and capture cross section above 100 eV based on experimental and sensitivity data analysis. The 36 criticalities of different size fast reactors were utilized for adjustment purposes [12]. The impact of the newly evaluated library on the new core design concept has not been conducted so far. Thus, the uncertainty propagation of the calculation result needs to be carefully estimated and presented in this study.

Two methods are used to propagate uncertainties from nuclear data to quantities of large-scale systems. The first method is the stochastic method (Monte Carlo method), which involves generating random samples based on probability distributions of input parameters (e.g., cross-sectional data and model parameters) and propagating these samples through a computational model to estimate output uncertainties. This method relies on a large number of calculations [15]. The second method is the deterministic method in which both sensitivity profiles and covariance data need to be combined to obtain the final uncertainty, and the sandwich formula is widely used to quantify the uncertainty in this case. The major advantages of using the deterministic method to propagate the calculation errors are as follows: (i) if all sensitivities are available, then all of the objectives of sensitivity analysis can be pursued efficiently; and (ii) since the response sensitivities and parameter uncertainties are obtained separately from each other, improvements in parameter uncertainties can immediately be propagated to improve the uncertainty in the response, without the need for expensive model recalculations [16]. The formula is particularly useful when dealing with correlated uncertainties and can provide more realistic estimates compared with other methods, especially in cases where the correlations between different nuclear reactions are significant. The uncertainties U (or $\sqrt{\sigma_R^2}$ $\sqrt{\sigma_R^2}$) k_{eff}, control drum worth, and the kinetic parameters originated from ENDF/B-VIII.0 library and JENDL-5 were evaluated using the sandwich rule as follows:

$$U = \sqrt{\sigma_R^2} = \sqrt{S_R^T \cdot C_{\Sigma\Sigma} \cdot S_R} U = \sqrt{\sigma_R^2} = \sqrt{S_R^T \cdot C_{\Sigma\Sigma} \cdot S_R}, \quad (1)$$

where S_R S_R is the sensitivity coefficient of the response R (R can be k_{eff}, β_{eff}, l_{eff}, or λ_{eff}) and T indicates transpose. For the fast spectrum of the MHPR core, the ECCO 33-group energy structure was chosen for the sensitivity calculation of k_{eff}, β_{eff}, l_{eff}, and λ_{eff} using Serpent 2. In Serpent 2, sensitivity analysis was conducted based on a collision history approach [17]. Covariance matrices $C_{\Sigma\Sigma}$ $C_{\Sigma\Sigma}$, which are evaluated by error propagations from experimental data, or the model parameters to the cross sections were retrieved from the JENDL-5/ENDF/B-VIII.0 database and processed into a 33-group energy structure using the ERROR module of NJOY21. The calculation algorithm flowchart for uncertainty quantification of ENDF/B-VIII.0/JENDL-5 using Serpent 2 is demonstrated in Figure 5.

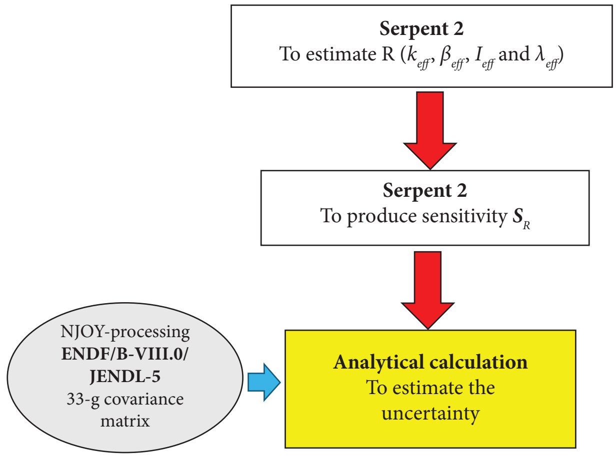

Figure 5: Calculation algorithm flowchart for uncertainty quantification of ENDF/B-VIII.0 and JENDL-5.

4. Eigenvalue Calculation Results and Uncertainty Analysis

The eigenvalue calculations of MHPR were conducted using Serpent 2 for both ENDF/B-VIII.0 library and JENDL-5, and the results are listed in Table 2. The core has k_{eff} at the beginning of the cycle (BOC) of 1.04909 ± 0.00013 for ENDF/B-VIII.0 and 1.05660 ± 0.00014 for JENDL-5. k_{eff} obtained by JENDL-5 is slightly larger than the one of ENDF/B-VIII.0 (about 270 pcm). In JENDL-5, the neutron reaction data for a large number of nuclei in the previous version (JENDL-4.0) were intensively updated and more nuclei of neutron reaction data were stored, which affected nuclear reactor calculations. The fission cross sections of $^{233,235,238}U$ and ^{239,240,241}Pu for fast neutrons were fully updated by the simultaneous evaluation extending the energy upper limit to 200 MeV. The resonance parameters of ^{235}U adopted ENDF-B/VIII.0 with a minor adjustment on the cross sections above 100 eV based on fast reactor benchmark tests. The prompt fission neutron spectra below 5 MeV were newly evaluated by model-based fitting to the available experimental data. For ^{238}U and ^{239}Pu, the resonance parameters of ENDF/B-VIII.0 were adopted with some adjustments. Regarding ^{238}U capture and fission cross section, significant adjustments were made in the hundreds of eV energy range. A rather smooth and higher prompt neutron multiplicity of ^{239}Pu fission was observed using JENDL-5. As a result, the criticalities of the fast reactors were affected by these revisions [12] and it is considered to have caused the difference observed in the results of two libraries.

The control drum worth was calculated using equation (2) to investigate the effect of the control drum during core shutdown.

$$\text{Control rod worth (pcm)} = \left(\rho_{\text{drumin}} - \rho_{\text{drumout}}\right) \times 100000,$$
$$\text{Control rod worth (pcm)} = \left(\rho_{\text{drumin}} - \rho_{\text{drumout}}\right) \times 100000, \tag{2}$$

where ρ_{drumin} ρ_{drumin} is the reactivity with the control drum in and ρ_{drumout} ρ_{drumout} is the reactivity with the control drum out.

The worth of each control drum is 1686.6 ± 2.4 and 1648.7 ± 2.3 pcm for ENDF/B-VIII.0 and JENDL-5, respectively.

The fuel temperature coefficient is the primary temperature input parameter in nuclear safety as it immediately regulates the core's reactivity as temperature increases. The fuel temperature coefficient and monolith temperature coefficient can be calculated using the following equation:

$$\alpha = \frac{\Delta\rho}{\Delta T} = \frac{\rho_2 - \rho_1}{T_2 - T_1}\,\alpha = \frac{\Delta\rho}{\Delta T} = \frac{\rho_2 - \rho_1}{T_2 - T_1}, \tag{3}$$

where ρ_2 ρ_2 is the final reactivity, ρ_1 ρ_1 is the initial reactivity, T_2 T_2 is the final fuel/monolith temperature, and T_1 T_1 is the initial fuel/monolith temperature.

The MHPR has negative feedback with increasing temperature of fuel materials, even though the negativity is relatively small (−0.1032 and −0.083 cents/K with uncertainty of 0.0003 and 0.0006 for JENDL-5 and ENDF/B-VIII.0, respectively). This is predictable since Doppler's effect is minor in the high-enriched uranium-fuelled monolithic reactor. The monolith feedback coefficient was found to be negligible as well.

Burnup calculations were carried out using JENDL-5 and ENDF/B-VIII.0 libraries and are depicted in Figure 6. As shown in Figure 6, the reactor core can operate at full power for 12 years without fuelling.

The total effective delayed neutron fraction β_{eff}, neutron generation time l_{eff}, and delayed neutron precursor decay constant λ_{eff} are important neutronics safety parameters and affect reactor control through the value of the reactor period. As shown in Table 2, the calculated β_{eff}, l_{eff}, and λ_{eff} are consistent for two libraries. The β_{eff} values are 706.54 ± 3.29 pcm and 705.44 ± 3.10 pcm for ENDF/B-VIII.0 and JENDL-5, respectively. The l_{eff} values are $0.1642 \pm 0.0009\,\mu$s and $0.1711 \pm 0.0010\,\mu$s, and λ_{eff} values are $0.509 \pm 0.004\,\text{s}^{-1}$ and $0.478 \pm 0.005\,\text{s}^{-1}$ for ENDF/B-VIII.0 and JENDL-5, respectively. Using the Inhour equation, the reactor period can be calculated [18] as follows:

Table 2: Core parameters at BOC of MHPR obtained by Serpent 2.

Parameters	ENDF/B-VIII.0		JENDL-5	
	Value	Uncertainty	Value	Uncertainty
k_{eff}	1.04909 ± 0.00013	678.52 (pcm)	1.05126 ± 0.00014	525.91 (pcm)
Control drum worth (pcm)	1686.6 ± 2.4	34.92	1648.7 ± 2.3	40.89
Fuel feedback coefficient (cents/K)	−0.0834	0.0003	−0.1032	0.0006
Monolith feedback coefficient (cents/K)	0.0089	0.0003	−0.0815	0.0005
β_{eff} (pcm)	706.54 ± 3.29	4.14	705.44 ± 3.10	5.69
l_{eff} (μs)	0.1642 ± 0.0009	0.0020	0.1711 ± 0.0010	0.0013
λ_{eff} (s^{-1})	0.509 ± 0.004	0.0069	0.478 ± 0.005	0.0041

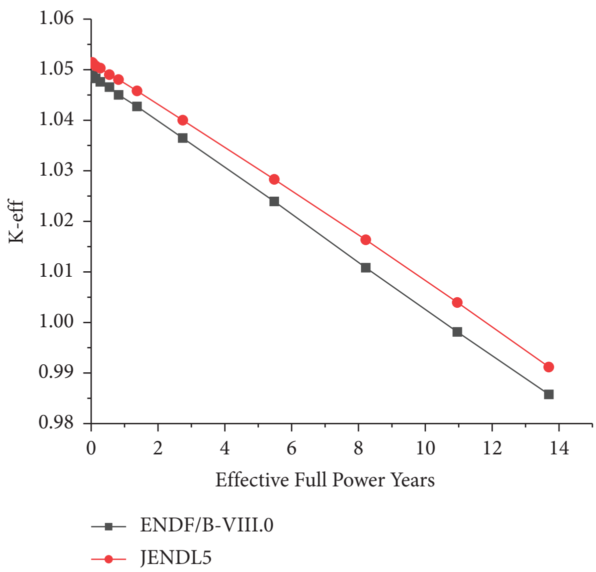

Figure 6: Evaluation of k_{eff} due to burnup years obtained by Serpent 2 using JENDL-5 and ENDF/B-VIII.0.

$$T = \frac{l_{eff}}{\rho} T = \frac{l_{eff}}{\rho}, \quad (4)$$

where ρ ρ is reactivity and l_{eff} l_{eff} was obtained as $l_{eff} = l + \beta_{eff} - \rho/\lambda_{eff}$ $l_{eff} = l + \beta_{eff} - \rho/\lambda_{eff}$ with l is the prompt neutron generation time. The difference in those kinetic parameters between ENDF/B-VIII.0 and JENDL-5 results in the reactor period of JENDL-5 being 1.042 times larger than that of ENDF/B-VIII.0, which will not have a significant impact on reactor operation safety.

The k_{eff} is an important parameter in safety analysis for the reactor, and the impact of nuclear data uncertainty on reactor safety margins comes principally from uncertainty in criticality [19]. The uncertainty was quantified for all isotopes in the material composition of the MHPR except for the ones lacking of C_Σ C_Σ on the database of ENDF/B-VIII.0 and JENDL-5. Uncertainties originated from cross sections, the average number of neutrons per fission—total ν, and angular distributions were taken into account. There is no target accuracy of k_{eff} for microsize reactors yet, but for fast reactors in general, the design target accuracy of k_{eff} is set to 300 pcm [20]. In comparison with this value, the total uncertainties of k_{eff} were found to be significant for both libraries: 678.52 pcm for ENDF/B-VIII.0 and 525.91 pcm for JENDL-5. The statistical error of k_{eff} is small (less than 14 pcm) compared with the total uncertainty. Thus, its contribution to the total uncertainty can be neglected. The sensitivity of the control drum worth was derived from the sensitivity of $k_{eff,}$ and the error was propagated. Uncertainty of control drum worth is less than 40 pcm for two libraries.

For breakdown information, the most significant contributors of k_{eff} uncertainty are listed in Table 3. As shown in Table 3, in the ENDF/B-VIII.0's case, the uncertainty of k_{eff} mostly came from ^{235}U total ν (409.18 pcm), fission cross section (327.24 pcm), and capture cross section (248.84 pcm). The next contributors for ENDF/B-VIII.0 are capture reactions of ^{16}O (243.57 pcm), ^{238}U (147.53 pcm), ^{56}Fe (138.38 pcm), and ^{238}U total ν (106.01 pcm). Other contributors with uncertainty of less than 100 pcm are summarized in Table 3. Compared to ENDF/B-VIII.0, the uncertainty of k_{eff} originated from ^{235}U total ν of JENDL-5 is much smaller (148.93 pcm). Sensitivities of k_{eff} were obtained directly from Serpent 2 output, and the sensitivity per unit lethargy is plotted in Figure 7 with neutron lethargy (u) being the logarithmic energy decrement ($\ln(E/E')$), where E and E' are the energy bins of one energy group. The similarity in group-wise structured sensitivities is observed for two libraries. The difference is mainly due to the difference in covariance matrices. The 33-group covariance matrices of major contributors to the total uncertainty of k_{eff} for ENDF/B-VIII.0 library and JENDL-5 including ^{235}U total ν, ^{235}U, ^{16}O, ^{56}Fe, and ^{238}U capture cross sections are depicted in Figure 8. As we can see from the figure the total ν of ^{235}U, ENDF/B-VIII.0 library with a much larger covariance matrix results in a much larger uncertainty. In the case of ^{235}U fission reaction cross section, the sensitivities of two libraries have peaks at hundreds of keV, and the larger covariance matrix of ENDF/B-VIII.0 at the same energy range leads to higher uncertainty than that of JENDL-5. The larger uncertainty in the fast energy region of ENDF/B-VIII.0 library causes higher uncertainties for the capture reaction cross section of ^{235}U, ^{16}O, and ^{238}U compared with that of JENDL-5. ^{56}Fe is the largest composition in the heat pipe reactor, and the uncertainty originating from ^{56}Fe capture cross section was found to be the largest contributor for JENDL-5 (361.93 pcm). The sensitivity of the ^{56}Fe capture cross section has the largest value in the thermal range. Thus, the larger covariance matrix of the reaction of ENDF/B-VIII.0 in the fast range does not lead to larger uncertainty in this case. The relatively high covariance matrix of JENDL-5 range combined with the high sensitivity at low energy results in

Table 3: Contributions to uncertainty in k_{eff} for MHPR from Serpent 2 at BOC.

Nuclear data	Uncertainty (pcm)	
	ENDF/B-VIII.0	JENDL-5
^{235}U total/^{235}U total	409.18	148.93
$^{235}U(n, f)/^{235}U(n, f)$	327.24	191.71
$^{235}U(n, \gamma)/^{235}U(n, \gamma)$	248.84	113.77
$^{16}O(n, \gamma)/^{16}O(n, \gamma)$	243.57	139.77
$^{238}U(n, \gamma)/^{238}U(n, \gamma)$	147.53	167.33
^{56}Fe$(n, \gamma)/^{56}$Fe(n, γ)	138.38	361.93
^{238}U total/^{238}U total	106.01	53.05
^{4}He elastic/^{4}He elastic	70.91	—
$^{238}U(n, f)/^{238}U(n, f)$	64.16	53.36
^{56}Fe elastic/^{56}Fe elastic	30.09	65.66
^{56}Fe angular distribution	—	46.37
^{52}Cr elastic/^{52}Cr elastic	22.33	13.80
^{238}U inelastic/^{238}U inelastic	21.70	85.01
^{16}O elastic/^{16}O elastic	19.66	25.45
^{238}U elastic/^{238}U elastic	18.45	28.76
^{16}O angular distribution	—	14.73
^{238}U angular distribution	—	12.50

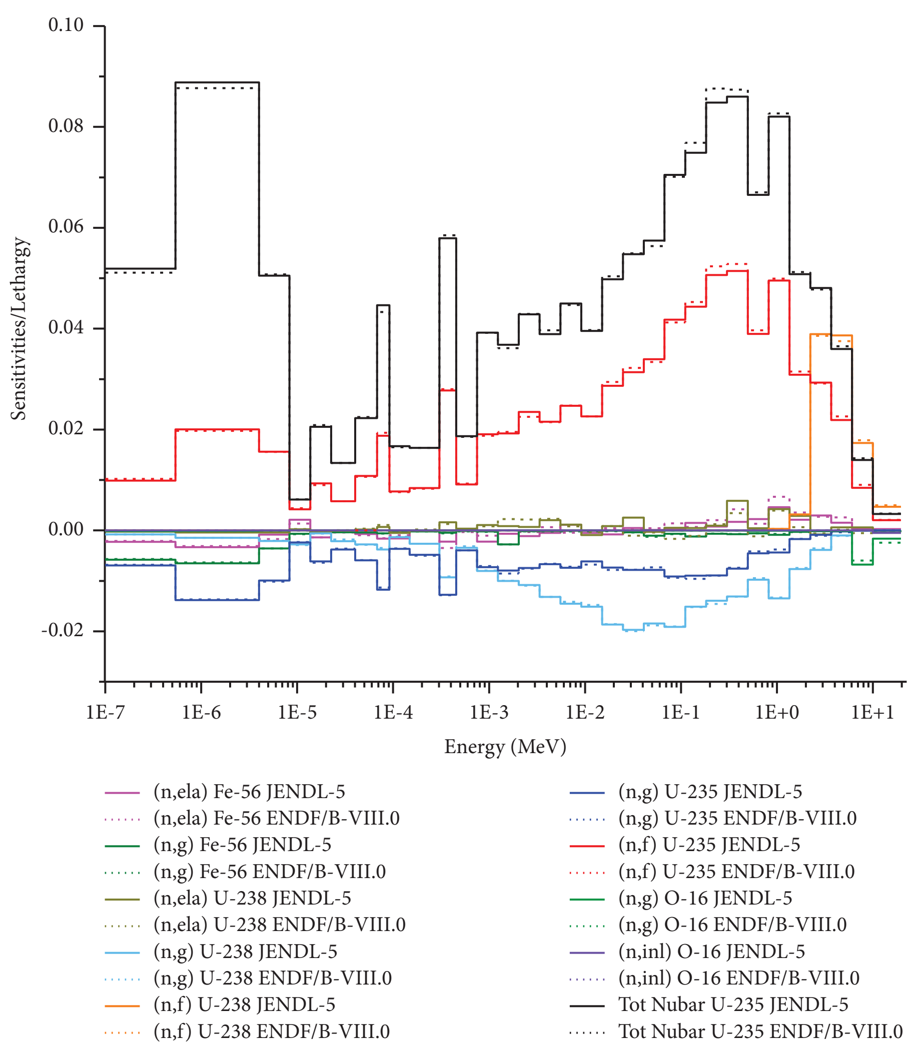

Figure 7: Energy-dependent sensitivity profile of k_{eff} of significant isotopes with BOC composition.

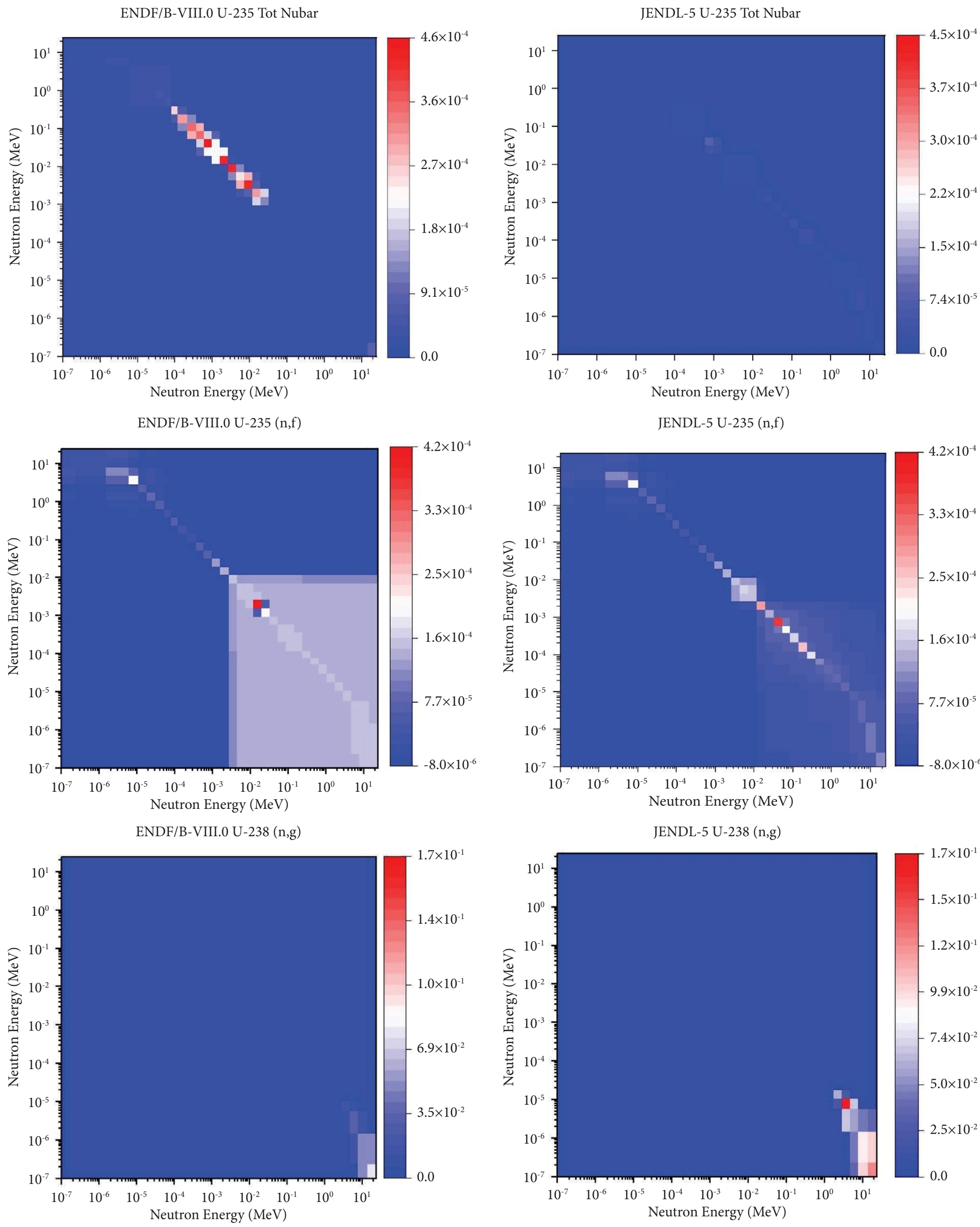

(a)

Figure 8: Continued.

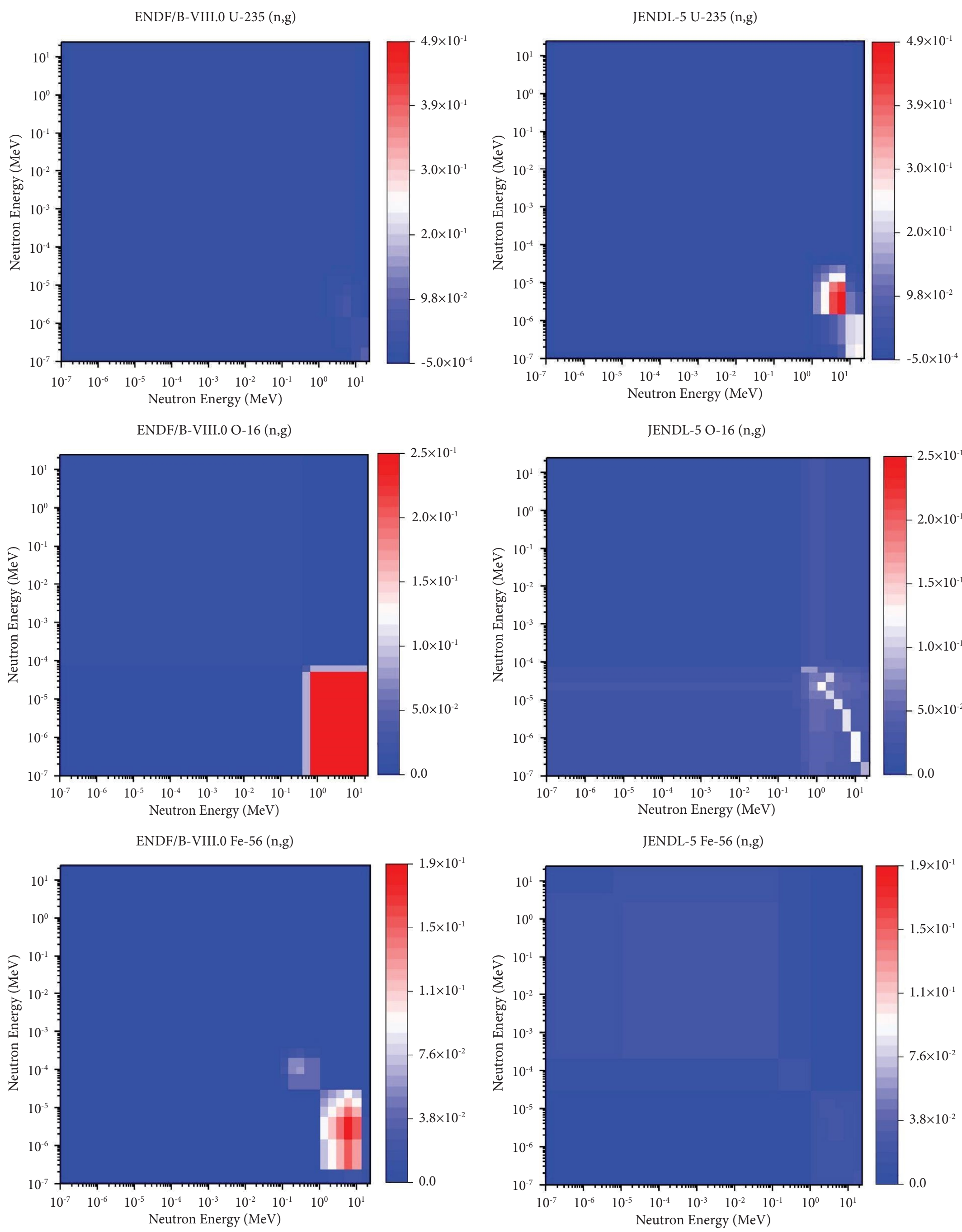

(b)

Figure 8: Covariance matrices of ^{235}U total ν, ^{235}U fission, ^{238}U, ^{235}U, ^{16}O, and ^{56}Fe capture cross sections of ENDF/B-VIII.0 and JENDL-5 libraries. (a) Covariance matrices of ^{235}U total ν, ^{235}U fission and ^{238}U capture cross sections, and (b) Covariance matrices of ^{235}U, ^{16}O, and ^{56}Fe capture cross sections.

a large k_{eff} uncertainty for JENDL-5. For microsize reactors where the neutron leakage can be significant, the uncertainty for angular distribution was also estimated. For uncertainty calculation of angular distribution, the covariance matrices retrieved from JENDL-5 and ENDF/B-VIII.0 also need to be processed into the 33-group structure using NJOY21. However, only 33-group covariance matrices of angular distribution from JENDL-5 can be obtained. Because of the setup of the covariance matrices for angular distribution in ENDF/B-VIII.0, 33-group covariance matrices were unable to be computed by NJOY21. Therefore, in this investigation, only the result of the total uncertainty of JENDL-5 is included in the angular distribution. Nevertheless, its contribution to total uncertainty is revealed to be not significant (total uncertainty with an angular distribution of 525.91 pcm and total uncertainty with an angular distribution of 523.45 pcm for

JENDL-5). The largest uncertainty from angular distribution was found for ^{56}Fe (46.37 pcm).

For kinetic parameters, the overall uncertainty of β_{eff} is only 4.14 pcm (0.59%) for ENDF/B-VIII.0 and 5.69 pcm (0.81%) for JENDL-5. Similarly, a considerably small total uncertainty of leff (0.85% for ENDF/B-VIII.0 and 1.15% for JENDL-5) and λeff (0.81% and 1.45% and 0.81%, respectively) were obtained. The uncertainties for those parameters are less than 1% for ENDF/B-VIII.0. For the latest library JENDL-5, the most significant contributor for β_{eff} uncertainty is the ^{238}U inelastic scattering cross section, for l_{eff} is the ^{56}Fe capture cross section, and for λ_{eff} is the ^{235}U elastic scattering cross section. With the uncertainties being about 1%, the impact of nuclear libraries such as ENDF/B-VIII.0 and JENDL-5 on those kinetic parameters can be considered to be minor.

5. Conclusions

Eigenvalue and kinetic parameters of the micro-size heat pipe core concept MHPR 10 $\mathrm{MW_{th}}$ were calculated using the latest library JENDL-5 and compared with the ENDF/B-VIII.0 library. The 270 pcm difference between the k_{eff} values of two libraries was taken into account in the revision of JENDL-5 in the fast region. The k_{eff} uncertainty due to total ν, reaction cross sections, and angular distribution was propagated, and by comparing with the target accuracy, it was found to be significant for both recently evaluated nuclear data libraries (678.52 pcm for ENDF/B-VIII.0 and 525.91 pcm for JENDL-5), and the largest contributors for ENDF/B-VIII.0 were ^{235}U total ν (409.18 pcm), while ^{56}Fe capture cross section (361.93 pcm) is the largest one in the case of JENDL-5. The similarity in group structure sensitivities of two libraries was observed, and thus, the difference in covariance matrices results in a difference in the evaluated k_{eff} uncertainty. For the kinetics parameter's uncertainty, the impact on the total β_{eff}, l_{eff}, and λ_{eff} simulation results was found to be minor. From the findings of this research, for similar fast microsize heat pipe reactor designs, it is essential to take into account the 600 pcm uncertainty of k_{eff} from ENDF/B-VIII.0/JENDL-5 libraries when discussing the neutronics performance and safety margin of the reactor core. In addition to that, with a smaller uncertainty in simulation results, JENDL-5 could provide a more reliable calculated k_{eff} of the reactor core.

Data Availability

The data will be provided for verification purposes.

Conflicts of Interest

The authors declare that they have no known conflicts of financial interests or personal relationships that could have appeared to influence the work reported in this paper.

Acknowledgments

This research was supported by the Office of Vice Chancellor for Research and Graduate Studies, University of Sharjah, UAE, under grant no. 230204082261. The authors would like to express their gratitude to Dr. Donny Hartanto, Salman Buti Al Aryani, and Mohammed Ahmed Mohammed for sharing resource and support.

References

[1] B. H. Yan, C. Wang, and L. G. Li, "The technology of micro heat pipe cooled reactor: a review," *Annals of Nuclear Energy*, vol. 135, Article ID 106948, 2020.

[2] W. Wits, "Heat Pipe nl Nederlands kenniscentrum voor heat pipe technologie Dutch knowledge center for heat pipe technology [Online Picture]," 2021, https://www.heatpipe.nl/index.php?page=heatpipe&lang=EN.

[3] P. McClure, D. Poston, V. Dasari, and R. Reid, "Design of megawatt power level heat pipe reactors," *Report of Los Alamos National Laboratory*, 2015.

[4] J. Sterbentz, J. Werner, A. Hummel et al., *Preliminary Assessment of Two Alternative Core Design Concepts for the Special Purpose Reactor*, Idaho National Lab.(INL), Idaho Falls, ID, USA, 2017.

[5] D. M. Castelluccio, G. Grasso, F. Lodi, V. Peluso, and A. Mengoni, "Nuclear data target accuracy requirements for advanced reactors: the ALFRED case," *Annals of Nuclear Energy*, vol. 162, Article ID 108533, 2021.

[6] P. Romojaro, F. Alvarez-Velarde, O. Cabellos, N. García-Herranz, and A. Jiménez-Carrascosa, "On the importance of target accuracy assessments and data assimilation for the Co-development of nuclear data and fast reactors: MYRRHA and ESFR," *Annals of Nuclear Energy*, vol. 161, Article ID 108416, 2021.

[7] G. Palmiotti and M. Salvatores, "Nuclear data target accuracy requirements for MA burners," *Transactions of the American Nuclear Society*, vol. 104, p. 681, 2011.

[8] T. M. Vu, D. Hartanto, T. N. Chu, N. V. H. Pham, and T. H. Bui, "Sensitivity and uncertainty analysis of neutronic and kinetic parameters for CERCER and CERMET fueled ADS using Serpent 2 and ENDF/B-VIII.0," *Annals of Nuclear Energy*, vol. 168, Article ID 108912, 2022.

[9] T. M. Vu and D. Hartanto, "Study on the sensitivity and uncertainty of nuclear data to the sodium-cooled linear breed-and-burn fast reactor using SCALE6.2. Code," *Science and Technology of Nuclear Installation*, Article ID 9997867, 2021.

[10] J. Leppanen, M. Pusa, T. Viitanen, V. Valtavirta, and T. Kaltiaisenaho, "The Serpent Monte Carlo code: status, development and applications in 2013," *Annals of Nuclear Energy*, vol. 82, pp. 142–150, 2015.

[11] D. A. Brown, M. B. Chadwick, R. Capote et al., "ENDF/B-VIII.0: the 8th major release of the nuclear reaction data library with CIELO-project cross sections, new standards and thermal scattering data," *Nuclear Data Sheets*, vol. 148, pp. 1–142, 2018.

[12] O. Iwamoto, N. Iwamoto, S. Kunieda et al., "Japanese evaluated nuclear data library version 5: JENDL-5," *Journal of Nuclear Science and Technology*, vol. 60, no. 1, pp. 1–60, 2023.

[13] Y. Nauchi and T. Kameyama, “Development of calculation technique for Iterated Fission Probability and reactor kinetic parameters using continuous-energy Monte Carlo method,” *Journal of Nuclear Science and Technology*, vol. 47, no. 11, pp. 977–990, 2010.

[14] B. C. Kiedrowski, “Impact of delayed neutron precursor mobility in fissile solution systems,” *Proceedings of PHYSOR 2012*, pp. 15–20, PHYSOR, Knoxville, TN, USA, 2012.

[15] D. Rochman, A. J. Koning, S. C. V. D. Marck, A. Hogenbirk, and D. V. Veen, “Nuclear data uncertainty propagation: total Monte Carlo vs. Covariances,” *Journal of the Korean Physical Society*, vol. 59, no. 2(3), pp. 1236–1241, 2011.

[16] D. G. Cacuci, M. Ionescu-Bujor, and I. M. Navon, *Sensitivity And Uncertainty Analysis: Applications To Large-Scale Systems*, CRC Press Taylor and Francis, Boca Raton, FL, USA, 2005.

[17] M. Aufiero, A. Bidaud, M. Hursin et al., “A collision history-based approach to sensitivity/perturbation calculations in the continuous energy Monte Carlo code Serpent,” *Annals of Nuclear Energy*, vol. 85, pp. 245–258, 2015.

[18] J. R. Lamarsh, *Introduction to Nuclear Reactor Theory*, Addison-Wesley Publishing Company, Massachusetts, MA, USA, 1966.

[19] J. N. Wilson, S. Siem, S. J. Rose et al., “Nuclear data for reactor physics: cross sections and level densities in the actinide region,” *EPJ Web of Conferences*, vol. 2, p. 12001, 2010.

[20] M. Salvatores, “Uncertainty and target accuracy assessment for innovative systems using recent covariance data evaluations,” *International Evaluation Co-operation*, vol. 26, 2008.